Atmos. Chem. Phys. Discuss., 5, 655–702, 2005
www.atmos-chem-phys.org/acpd/5/655/
SRef-ID: 1680-7375/acpd/2005-5-655
European Geosciences Union

Atmospheric Chemistry and Physics Discussions

Observations and model calculations of trace gas scavenging in a dense Saharan dust plume during MINATROC

M. de Reus[1], **H. Fischer**[1], **R. Sander**[1], **V. Gros**[1], **R. Kormann**[1], **G. Salisbury**[1], **R. Van Dingenen**[2], **J. Williams**[1], **M. Zöllner**[1], **and J. Lelieveld**[1]

[1]Max Planck Institute for Chemistry, PO Box 3060, 55020 Mainz, Germany
[2]Joint Research Centre, Ispra, Italy

Received: 13 January 2005 – Accepted: 31 January 2005 – Published: 11 February 2005

Correspondence to: M. de Reus (reus@mpch-mainz.mpg.de)

Abstract

An intensive field measurement campaign was performed in July/August 2002 at the Global Atmospheric Watch station Izaña on Tenerife to study the interaction of mineral dust aerosol and tropospheric chemistry (MINATROC). A dense Saharan dust plume, with aerosol masses exceeding 500 μg m^{-3}, persisted for three days. During this dust event strongly reduced mixing ratios of RO_x (HO_2, CH_3O_2 and higher organic peroxy radicals), H_2O_2, NO_x (NO and NO_2) and O_3 were observed. A chemistry boxmodel, constrained by the measurements, has been used to study gas phase and heterogeneous chemistry. It appeared to be difficult to reproduce the observed HCHO mixing ratios with the model, possibly related to the representation of precursor gas concentrations or the absence of dry deposition. The model calculations indicate that the reduced H_2O_2 mixing ratios in the dust plume can be explained by including the heterogeneous removal reaction of HO_2 with an uptake coefficient of 0.2, or by assuming heterogeneous removal of H_2O_2 with an accommodation coefficient of 3×10^{-4}. However, these heterogeneous reactions cannot explain the low RO_x mixing ratios observed during the dust event. Whereas a mean daytime net ozone production rate (NOP) of 1.06 ppb$_v$/hr occurred throughout the campaign, the reduced RO_x and NO_x mixing ratios in the Saharan dust plume contributed to a reduced NOP of 0.14–0.32 ppb$_v$/hr, which likely explains the relatively low ozone mixing ratios observed during this event.

1. Introduction

The interaction between atmospheric aerosols and photochemistry via heterogeneous reactions has been subject to intense investigation during the last decades. As an example, heterogeneous reactions on polar stratospheric clouds lead to the destruction of stratospheric ozone (e.g. Crutzen and Arnold, 1986). Heterogeneous reactions on cloud droplets and aerosols are also found to be important for tropospheric chemistry (e.g. Lelieveld and Crutzen, 1990). Special emphasis has been given to reactions on mineral dust aerosol (e.g. Usher et al., 2003), since these particles provide a large surface area for heterogeneous reactions in the troposphere (IPCC, 1996).

During several field campaigns a correlation between high dust loadings and low O_3 and HNO_3 concentrations has been observed (e.g. de Reus et al., 2000; Hanke et al., 2003; Bonasoni et al., 2004). The latter authors also showed that dust-poor airmasses originating in North Africa had significantly higher O_3 concentrations than those which carried dust.

Chemical boxmodels as well as global and regional chemical-transport models have been used to calculate the reduction in trace gas mixing ratios due to heterogeneous reactions on mineral dust aerosol. Most studies focussed on ozone and nitrogen species, while only a few studies report effects of mineral dust on OH and HO_2 mixing ratios. Zhang et al. (1994) and Zhang and Carmichael (1999), for example, used a box-model to simulate the loss of SO_2, NO_x, HO_2 and O_3 due to heterogeneous reactions on mineral dust aerosol. Dentener et al. (1996) performed simulations with a global chemistry-transport model and calculated an O_3 reduction up to 10% in and nearby dust source areas. De Reus et al. (2000) calculated a 30–40% reduction of O_3 in a Saharan dust plume near the coast of Africa, attributed to the direct removal of O_3 by dust aerosol and the heterogeneous removal of HNO_3. Bauer et al. (2004) calculated a 5% reduction in global tropospheric ozone and concluded that this was mainly due to the uptake of HNO_3 on dust aerosol and not due to the direct uptake of O_3. However, the HNO_3 concentration was overestimated by the global model, which may have strongly biased the results of this study. Bian and Zender (2003) investigated the effect of reduced photolysis rates and heterogeneous chemistry on the tropospheric trace gas mixing ratios. They concluded that both processes cause a combined decrease in global mean O_3 of 0.7%, and 11.1% for OH, 5.2% for HO_2 and 3.5% for HNO_3. The effects of heterogeneous removal reactions clearly dominated over the reduced photolysis rates. Tang et al. (2004) performed a model study using a regional-scale chemistry-transport model and compared the results with aerosol chemical composition measurements in a dust plume encountered during the ACE-Asia measurement campaign. They investigated both the reduction in solar (actinic) radiation and heterogeneous reactions on the dust aerosol. Low O_3 concentrations in the dust plume could only be explained by heterogeneous reactions. It was inferred that the reduction of photolysis rates largely determines changes in OH concentrations, whereas the large decrease in HNO_3 (up to 95%) and SO_2 (up to 55%) concentrations was due to heterogeneous reactions.

Although all aforementioned studies indicate a strong influence of mineral dust aerosols on tropospheric chemistry, the results are very different. This is mainly due to the large uncertainty in the uptake coefficients for the different trace gases on mineral dust aerosols. Moreover, for boxmodel calculations it has proven difficult to provide realistic initial conditions, and for regional and global models the comparison with observations appears to be a main limitation.

In this study we use an alternative approach. We employ a chemical boxmodel to analyse measurements performed within a dense Saharan dust plume at the Izaña observatory on Tenerife, Canary Islands. We use the model to calculate the steady state concentrations of RO_x, H_2O_2 and HCHO and compare them with observed values. For the model initialisation measured quantities are used to the extend possible. In addition to heterogeneous O_3 and HNO_3 uptake and the reduction of photolysis rates by mineral dust aerosol, as addressed in previous studies, we focus on the effects of HO_2 and H_2O_2 uptake in this study. Furthermore, we compare the net ozone production rate in the Saharan dust plume with airmasses not containing dust.

2. The MINATROC experiment

The MINATROC (MINeral dust And TROpospheric Chemistry) project was designed to investigate the effects of heterogeneous reactions involving mineral aerosol on tropospheric chemistry. The project combined three types of research activities: laboratory experiments to quantify selected interactions between trace gases and mineral dust aerosol, field experiments to study the influence of mineral dust on tropospheric chemistry under realistic conditions, and global model studies to put the results of the former two into perspective. In this paper we will present observations of the second field experiment, performed in July/August 2002 at the Izaña observatory on the island of Tenerife, Spain.

Izaña observatory is part of the World Meteorological Organisation (WMO) Global Atmospheric Watch (GAW) network, and is operated by the Spanish Meteorological Institute. The station is situated on a mountain ridge on the island of Tenerife at 2360 m above sea level (a.s.l., 28°18′ N, 16°29′ W). Between 15 July and 15 August 2002 intensive aerosol and trace gas measurements were performed. The influence of mineral dust on the chemistry of the troposphere could be studied extensively during this period, since, besides several smaller dust episodes, a major dust event was probed between 28 and 31 July 2002.

3. Instrumentation

Additional to the set of measurements of the global watch program at Izaña, intensive measurements of aerosols and trace gases were performed during MINATROC by different institutes.

The instruments to measure atmospheric trace gases were operated by the Max Planck Institute for Chemistry, Mainz, Germany, from two laboratory containers. A sample air inlet was placed at the roof of both containers about 4 m above the ground. The RO_x instrument and the upward looking JNO_2 and JO^1D filter radiometers were deployed directly on the roof of the container at about 3 m above ground level, while the downward looking JNO_2 and JO^1D filter radiometers were mounted at a height of 1.5 m above ground level.

Table 1 lists the trace gas instruments which are relevant for this study, together with their associated uncertainties and detection limits. Since most instruments are similar to the ones which have been used during the first MINATROC field experiment at Mt. Cimone in June 2000, a detailed description of the O_3, CO, RO_x, NO and NO_y

instruments can be found in Fischer et al. (2003). For the other instruments more details are given below.

A liquid chemistry fluorescence detector (AERO laser model AL 4021) was used to measure formaldehyde (HCHO). The instrument first strips the HCHO from the ambient air into a strongly diluted H_2SO_4 solution, after which it reacts with acetylacetone and ammoniumacetate to form 3,5-diacetyl-1,4-dihydrolutidine (DDL) following the Hantzsch reaction. The fluorescence signal of the excited reaction product is detected by a photomultiplier at 510 nm. The same instrument has been employed during a previous aircraft campaign (Kormann et al., 2003).

For the determination of H_2O_2 a second liquid chemistry fluorescence detector has been used (AERO laser model AL 2001CA). After stripping H_2O_2 from the ambient air in a slightly acidic solution, this instrument determines the total peroxide concentration by the liquid phase reaction of peroxides with p-hydroxyphenylacetic acid, catalysed by peroxidase. To distinguish between H_2O_2 and organic peroxides two parallel channels are used. In one channel H_2O_2 is selectively destroyed by catalase prior to the fluorescence detection in the instrument. The difference between the signals from both channels is a measure for the H_2O_2 concentration (Lazrus et al., 1986).

No quantification of organic peroxides can be achieved without knowing the specific peroxide composition in the atmosphere. This is due to the high variability in the relative amounts of peroxides in ambient air, the large variations in Henry's law constants, and, consequently, the collection efficiencies for these compounds. However, if we assume that the most abundant organic peroxide in the atmosphere is methylhydroperoxide (MHP, CH_3OOH) and that the collection efficiency of MHP is 60%, an upper limit for the MHP mixing ratio can be determined. The obtained CH_3OOH mixing ratio should, however, be interpreted with considerable care.

The calibration of both AL detectors was carried out both in the gas and the liquid phase. HCHO calibration gas was produced using a VICI Metronics permeation tube operated at a temperature of 80°C, while for H_2O_2 a home-built permeation device was used, consisting of a semi-permeable polyethylene tube which was placed in a saturated H_2O_2 environment (glass bottle with a small amount of 30% H_2O_2 solution, operated at a constant temperature of 30°C). Zero air (CAP60 Headline Filters air purifier) with a total flow of 6 L/min was mixed with the calibration gas stream leading to a mixing ratio of 13.3 ppb_v HCHO and 5.9 ppb_v H_2O_2. Every 4–6 h calibration gas was added to the sample air at the top of the sample mast, to determine the losses of HCHO and H_2O_2 in the inlet line. To test the stability of the instrument, additional liquid calibrations were performed once a day with 1 μM HCHO and H_2O_2 solutions.

Measurements of a range of volatile organic carbons (VOC) were performed using a proton-transfer-reaction mass spectrometer (PTRMS). Inside this instrument organic species are chemically ionised by the proton transfer with H_3O^+ ions and the products are detected with a quadrupole mass spectrometer (Lindinger et al., 1998). In this study the measurements of acetone, methanol and isoprene are used. The isoprene mixing ratios measured with the PTRMS, however, should be regarded as upper limits, due to other possible contributions to this mass (Williams et al., 2001). More details about the measurement technique and calibration procedure can be found in Salisbury et al. (2003).

For the measurement of non methane hydrocarbons (NMHC) stainless steel canister samples were taken every 3 or 6 h during the campaign, which were analysed in the laboratory of the Max Planck Institute in Mainz, using a gas chromatograph–mass spectrometer system (GC-MS). Due to the set-up of the GC-MS system only hydrocarbons with more than 3 C atoms were analysed. More details about the collection of the samples, the GS-MS system and its calibration procedure can be found in Gros et al. (2003).

Aerosol measurements were performed from a mobile laboratory by the Joint Research Centre, Ispra, Italy. Dry aerosol size distributions in the size range 6–600 nm diameter were measured with a custom built Vienna type differential mobility analyser (DMA), using a TSI CPC model 3010 as particle counter (Thermo Systems Inc. Condensation Particle Counter). The number size distribution of coarse particles was determined with an Optical Particle Counter (OPC, GRIMM model 1.108) in 15 size classes from 300 nm to 10 μm diameter. Note that the aerosols entering the OPC have not been dried, however, for the low relative humidities (<60%) observed during the campaign, the observed aerosol diameter can be regarded as dry diameter. Combining the data of both instruments provides the aerosol size distribution between 6 nm and 10 μm diameter, from which the total aerosol surface area and volume was calculated. Total PM10 (particle diameter (D_p)<10 μm) aerosol mass was obtained on-line with a tapered element oscillating microbalance (TEOM) system, with a total uncertainty of ±15%.

4. Meteorology

The synoptic situation over the Canary Islands is usually dominated by a subtropical anticyclone, centred over the Azores (Carslaw et al., 1997). Deviations in the position of this anticyclone generally determine the origin of the airmasses observed at the Izaña observatory. During the MINATROC campaign in July/August 2002 four regions of origin could be identified based on backtrajectories calculated with the HYSPLIT model (HYbrid Single-Particle Lagrangian Integrated Trajectory, http://www.arl.noaa.gov/ready/hysplit4.html): north Atlantic, central Atlantic, tropical Africa and the Sahara region.

Several time periods with airmasses containing mineral dust, originating in the Sahara region and tropical Africa could be identified. The strongest Saharan dust plume was observed between 28 and 31 July. Aerosol index images from the TOMS satellite indicate that this dust plume originated in western Algeria and its border region with Mali and Mauritania. Backtrajectory calculations suggest that the airmasses were lifted from between 500 and 1500 m above ground level to the measurement altitude of about 2.5 km, 2.5 to 3 days before arrival at the Izaña measurement station, and originate more to the southwest in Mauritania. Lidar measurements indicate that the Saharan dust plume extended to an altitude of about 7 km (G. P. Gobbi, personal communication, 2003).

5. Observations

The mixing ratios of a selection of trace gases together with the observed temperature, relative humidity, aerosol number concentration and aerosol surface area are shown in Fig. 1. Continuous in-situ measurements were performed between 16 July and 15 August 2002. Due to instrument calibrations some short gaps occur in the dataset. A delay in the analytic gas shipment to the measurement station precluded RO_x measurements between 22 July and 29 July. Moreover, due to inlet problems no reliable measurements of acetone, methanol, isoprene and NMHC could be obtained before 29 July. The dataset has been reduced to 30 min averaged values, except for the aerosol mass concentrations for which only hourly averages are available.

Figure 2 shows the average diurnal cycle for a selection of species observed during the campaign. A strong diurnal cycle was observed for most trace gases and the aerosol number concentration. This is mainly driven by local air circulation patterns at the measurement site, which are typical for a high-elevation mountainous site. During daytime the air flows upward to the sampling site resulting from surface warming (upslope winds), while downslope winds are observed during the night, due to cooling of the mountain slopes (Zaveri et al., 1995). As a result, free tropospheric air masses were observed during the night (21:00–07:00 UTC) and airmasses influenced by anthropogenic pollution from the local boundary layer during the day (07:00–21:00 UTC).

The fraction of boundary layer air which has been mixed into the free tropospheric airmasses at the measurement station has been estimated using relative humidity profiles obtained by radiosondes launched in Santa Cruz, the capital of Tenerife, situated at the south-western coast of the island (Schultz, 1995). For this method three water vapour mixing ratios are used: (1) the H_2O mixing ratio measured at the Izaña station (H_2O_{izo}), (2) the H_2O mixing ratio measured by the radiosonde in the free troposphere at the same altitude as the measurement station (H_2O_{FT}) and (3) the H_2O mixing ratio measured by the radiosonde in the marine boundary layer at 100m asl. (H_2O_{MBL}). The mixing factor can then be defined as: $(H_2O_{izo}-H_2O_{FT})/(H_2O_{MBL}-H_2O_{FT})$. Since only two radiosondes were launched per day only one instantaneous daytime value for the mixing factor could be obtained per day. The daytime mixing factor ranged between −30 and 65% and had a median value of 17% in the dust-poor airmasses. During the major dust event the measurements were less influenced by local pollution, the median mixing factor during the dust event was 0.8%.

For CO, NO_x, methanol, acetone and aerosols the upslope winds resulted in an enhancement of the concentrations during the day, due to the intrusion of anthropogenic pollution from the boundary layer. On the other hand O_3 and H_2O_2 mixing ratios were lower during the day, as a result of their positive vertical gradients in the lower atmosphere, mainly due to enhanced destruction of these species by dry deposition at the surface. The RO_x and HCHO mixing ratios closely followed the solar radiation intensity. For these shorter lived species the diurnal variation is less affected by transport and much more dependent on local photochemical production, maximizing around local noon.

For a statistical analysis of the data, upslope and downslope conditions have been separated. Upslope conditions could be identified by a strong enhancement in aerosol number concentration and occurred between 07:00 and 21:00 UTC (daytime), downslope conditions correspondingly between 21:00 and 07:00 UTC (nighttime). Average daytime and nighttime values for the observed trace gas mixing ratios and aerosol number concentration, surface area, volume and mass are listed in Table 2.

Table 2 and Fig. 2 also distinguish airmasses containing dust from those which were not influenced by dust. During the measurement campaign several Saharan dust events were probed with PM10 aerosol mass concentrations exceeding 25 $\mu g\ m^{-3}$. The most pronounced dust event was probed between 28 July, 16.45 UTC and 31 July, 15.15 UTC, when aerosol mass concentrations up to 500 $\mu g\ m^{-3}$ were observed, and the aerosol optical thickness reached values of 0.95. In air masses which were not influenced by Saharan dust, these values were below 10 $\mu g\ m^{-3}$ and 0.5, respectively. For the analyses in this paper we focus on this major dust event and treat the minor dust events as "dust-poor" airmasses. The time period of the Saharan dust event has been marked by a grey box in Fig. 1.

Some of the observed trace gases show a distinct change during the dust event. The most pronounced is the decrease in ozone mixing ratio from about 65 ppb_v just before the dust event started to below 35 ppb_v during the dust event (ppb_v=nmol/mol). At the same time relatively low H_2O_2 mixing ratios were observed. In free tropospheric air masses (nighttime), an average H_2O_2 mixing ratio of 0.61±0.25 ppb_v was observed during the dust period, whereas it was 1.72±0.55 ppb_v during the rest of the campaign. Also Fig. 2 depicts significantly lower O_3 and H_2O_2 mixing ratios in airmasses containing dust compared to dust-poor air. Unfortunately no RO_x measurements were available for the first half of the dust period, although during the second part of the dust period lower RO_x peak values, i.e. 23 ppt_v at 30 July and 32 ppt_v at 31 July were observed compared to the dust-poor days (43±16 ppt_v). Moreover, a difference in NO_x mixing ratio was found between dust and dust-poor airmasses, which could be a result of the suppressed transport of boundary layer air to the measurement station during the dust event. During upslope conditions 0.17 ppb_v NO_x was found in the dust plume, while 0.26 ppb_v NO_x was observed in the dust-poor airmasses. An additional and possibly more significant effect may be the heterogeneous loss of HNO_3 and N_2O_5 on the dust particles, which indirecty deplete NO_x. The mean relative humidity during the Saharan dust episode was 35%, with peak values up to 60%. This is high compared to the relative humidity observed during the rest of the campaign.

Furthermore, no significant change in the HCHO and CO mixing ratio was observed. Overall, an inhibition of the VOC diurnal cycle could be observed, with enhanced mixing ratios during the night throughout the dust event, indicating a slightly altered local wind pattern. Although a strong decrease in the HNO_3 mixing ratio is expected in a mineral dust plume (e.g. Dentener et al., 1996) and observed by Hanke et al. (2003), no significant change in the NO_y mixing ratio was observed. This is due to the fact that the NO_y converter measures the sum of all gaseous nitrogen species and aerosol nitrate. Hence, the uptake of HNO_3 on mineral dust aerosol is not expected to show up in the NO_y measurements. Remarkably, the mean daytime aerosol number concentration is highest in the dust-poor airmasses, which may also be explained by a reduced mixing of boundary layer air in the dust plume. The much higher particle surface area and mass concentration observed during the dust event indicates a very different aerosol size distribution in the dust loaded airmasses, with a higher number of larger particles. The small particles are probably scavenged by the larger Saharan dust aerosols in the plume, reducing the total aerosol number concentration. The photolysis rates of O_3 and NO_2 are reduced in the dust plume due to the absorption and scattering of solar radiation by the dense aerosol. The average daytime JNO_2 photolysis rate decreased by 17% and JO^1D by 15% during the Saharan dust event compared to the rest of the campaign.

Another interesting observation is the very high CO and O_3 mixing ratios during the first two days of the measurement campaign, which could be attributed to long range transport of a biomass burning plume from large forest fires in Quebec, Canada, on 6–9 July 2002. During these two days CO mixing ratios as high as 290 ppb_v and O_3mixing ratios of 100 ppb_v were observed. Although very interesting, this period will not be further studied in this paper.

A comparison of the observed trace gas mixing ratios with observations made during the first MINATROC field campaign on Mt. Cimone in June 2000 (Fischer et al., 2003) is presented in Table 3. The Mt. Cimone station is situated at 2165 m a.s.l. on the highest mountain in the northern Italian Apennines (44°11′ N, 10°42′ E). Due to its location in southern Europe, the sampled airmasses represent European continental background conditions. Similar O_3 mixing ratios have been observed at both measurements sites, while the CO and NO_x mixing ratios were slightly lower at Izaña, indicative of a more remote site, though influenced by continental pollution. The HCHO mixing ratios observed at Izaña were, however, much lower than those observed at Mt. Cimone. The results from the MINATROC campaign are also compared with measurements at the Izaña observatory performed in July/August 1993 during the OCTA field campaign (Fischer et al., 1998). Compared to the measurements at the same site nine years earlier, slightly higher O_3 and NO_x mixing ratios and much lower HCHO and H_2O_2

mixing ratios were observed in 2002. This appears to be consistent with an upward O_3 trend observed downwind of western Africa (Lelieveld et al., 2004). The median nighttime CO mixing ratio in 2002 was 9 ppb$_v$ lower than that observed in 1993, in line with the observed CO trend of −0.92±0.15 ppb$_v$/yr in the northern hemisphere lower troposphere (Novelli et al., 2003). The observed RO_x mixing ratios were similar, taking into account the large uncertainty in the RO_x measurements.

6. Boxmodel calculations

To investigate photochemistry, net ozone production and the influence of Saharan dust aerosol on the mixing ratios of peroxy radicals, formaldehyde and hydrogen peroxide, model calculations were performed with the chemistry box model MECCA (Module Efficiently Calculating the Chemistry of the Atmosphere). The chemical reaction scheme has been adopted from von Kuhlmann et al. (2003) and includes detailed chemistry of organic species with up to four C-atoms and isoprene (Sander et al., 2004). The reaction rates have generally been adopted from the Jet Propulsion Laboratory (JPL) 2003 database (Sander et al., 2003). Heterogeneous removal reactions of HO_2 and H_2O_2 on mineral dust have been added to the chemical scheme, analogous to de Reus et al. (2000). In total 67 chemical species, 110 gas phase chemical reactions, 34 photolysis reactions and 2 heterogeneous removal reactions were included (see electronic supplement http://www.copernicus.org/EGU/acp/acpd/5/655/acpd-5-655-sp1.pdf).

The boxmodel has been employed by constraining the concentrations of relatively long-lived trace gases to the observed values, whereas the steady state concentrations of short-lived trace gases are calculated. Here, we focus on peroxy radicals, formaldehyde and hydrogen peroxide.

6.1. Input parameters

Since two sets of observations are available per hour, a model simulation is started every 30 min. Each simulation has been initialised with the observed temperature, pressure, O_3, CO, H_2O, NO, H_2O_2, CH_3OOH, acetone, methanol, isoprene, propane and butane mixing ratios, which are shown in Fig. 1. Short gaps for which data are missing have been filled through interpolation. HNO_3 is initialised using the observed NO_z mixing ratio (NO_z=NO_y-NO_x). Since NO_y also includes atmospheric aerosol nitrate, HNO_3 will likely be strongly overestimated during the dust event when NO_z is used as a proxy for HNO_3 (see Sect. 5). Therefore, HNO_3 is set to zero during the major Saharan dust event. For CH_4 and CO_2 background mixing ratios for the year 2002 of 1.75 and 372 ppm_v have been used, respectively. Since no measurements of ethane, ethene and propene were performed during MINATROC, the mixing ratios of these species were scaled to the observed propane mixing ratio using the mean daytime mixing ratios observed during a former campaign at Izaña in July/August 1993 (Fischer et al., 1998). During this campaign the mean ratios of ethane, ethene and propene to propane were 10, 0.6 and 0.2, respectively.

JO^1D and JNO_2 photolysis rates were measured during the campaign and have been used as reaction rates for the photolysis reaction of O_3 (to O^1D) and NO_2, respectively. Other photolysis rates have been calculated using the Tropospheric Ultraviolet-Visible (TUV, version 4.1) radiation model (Madronich and Flocke, 1998). For these calculations, the total ozone column measured with a Dobson spectrometer at the Izaña station has been used as input value, while default values for the SO_2, NO_2, cloud and aerosol optical depth were used. To account for cloud overpasses and the reduction of solar radiation due to the Saharan dust plume, the calculated photolysis rates have been scaled to the ratio of the measured to the calculated JNO_2 photolysis rates.

A model simulation has been performed for every 30 min data point during daytime hours (solar zenith angle<70°). The mixing ratios of the above listed trace gases, temperature, pressure and photolysis rates have been kept constant during each simulation, while the model was run for 10 days, to make sure that steady state was achieved. Since no VOC and NMHC data are available before 29 July, only the later part of the campaign has been analysed.

6.2. Gas phase chemistry

Before we performed model simulations for the MINATROC dataset, we first carried out some calculations to determine the time needed to reach steady state for different species. At local noon, a steady state peroxy radical mixing ratio is achieved within an hour, however, the model has to run for at least 6 h to reach a steady state HCHO concentration. At higher solar zenith angles it takes somewhat longer to attain steady state, whereas during the night a steady state RO_x and HCHO mixing ratio is not reached at all. Therefore, each model simulation continues for 10 days, to ensure that steady state is achieved, and the simulations are limited to time periods during which the solar zenith angle is less than 70°. In later sensitivity runs the model is also used to calculate the H_2O_2 mixing ratio. Also for this trace gas steady state is reached well within 10 days for zenith angles$<70^\circ$.

6.2.1. Reference run

The RO_x mixing ratio calculated by the model without heterogeneous chemistry, for the period 29 July to 15 August 2002, is shown in Fig. 3a. RO_x is the sum of HO_2, CH_3O_2, higher organic peroxy radicals with up to 4 C atoms and peroxy radicals formed during isoprene degradation. The main constituents of the modelled RO_x are HO_2 (60%), CH_3O_2 (18%) and the peroxy radicals from isoprene degradation (16%). The contribution of other higher organic peroxy radicals to the total RO_x is very small, on average $C_2H_5O_2$ contributes 0.06% to the total modelled RO_x, $C_2H_3O_3$ 5.6%, $C_3H_7O_2$ 0.01%, $C_3H_6O_2$ 0.17%, $C_3H_5O_3$ 0.08%, $C_4H_9O_2$ 0.02% and $C_4H_9O_4$ 0.003%. The RO_x mixing ratio is clearly overestimated by the model, and the mean ratio of the calculated to the observed RO_x mixing ratio (RO_x calc/obs) is 1.70.

Figure 3b shows the calculated and observed HCHO mixing ratios. The HCHO mixing ratios are also strongly overestimated by the model. The daytime maximum HCHO mixing ratio calculated by the model ranges between 1.5 and 7.5 ppb_v, while the observed values vary between 0.7 and 1.7 ppb_v. The mean ratio of the calculated to observed HCHO mixing ratio (HCHO calc/obs) equals 2.29, however, a good correlation can be found between the observed and calculated HCHO mixing ratios. When fitting a straight line through the data points, the correlation coefficient r is 0.80.

Possible reasons for the model overestimation of both the RO_x and HCHO mixing ratios could either be an underestimation of the observed HCHO and RO_x mixing ratios, an overestimation of the precursor gas concentrations, which are used as input for the calculations or unknown model errors. A comparison of the HCHO and RO_x mixing ratios with a previous measurement campaign at Izaña shows that the HCHO mixing ratios are a factor 2 lower than those observed nine years earlier, however, during this campaign the HCHO measurements were probably overestimated due to a spectral interference to CH_4 (Fischer et al., 1998). The RO_x mixing ratios are similar considering the large uncertainty in the RO_x measurements (see Table 3). The influence of the input concentrations of different precursor gases for HCHO and RO_x will be studied in the next section.

6.2.2. Sensitivity simulations

To investigate the effects of a range of model input parameters, several sensitivity studies have been performed in which the mixing ratio of one trace gas has been reduced by a factor two compared to the reference run. The results are summarised in Table 4.

The calculated RO_x mixing ratio is rather insensitive to the changes in the input mixing ratios of most trace gases, except for O_3 and H_2O, which are direct precursors of HO_2, and for isoprene, which is a main precursor for different organic peroxides. Since the organic peroxy radicals, not originating from isoprene, contribute only 6% to the total peroxy radical mixing ratio, changes in the higher hydrocarbon concentrations do not have a significant effect on the calculated RO_x mixing ratio.

The simulated HCHO mixing ratio is more variable, and especially sensitive to the input concentration of NO. A reduction of the NO mixing ratio by a factor 2 causes the HCHO mixing ratio to decrease by 33%. At low NO mixing ratios the production of HCHO mainly occurs via the reaction of HO_2 with CH_3O_2 and the subsequent photolysis of CH_3OOH, while at higher NO mixing ratios, the HCHO production is dominated by the faster reaction of CH_3O_2 with NO, leading to an enhanced production of HCHO.

The simulated HCHO mixing ratio is also sensitive to the input concentration of isoprene (21% reduction of HCHO when the isoprene mixing ratio is reduced with a factor 2), O_3 (10%), H_2O (7%) and CH_3OOH (5%). Isoprene and CH_3OOH are precursor gases of HCHO, so a reduction in the mixing ratio of these trace gases will directly result in a reduced HCHO production. O_3 and H_2O influence the HCHO mixing ratio through the change in OH mixing ratio. If the concentration of O_3 or H_2O is reduced, less OH is produced via the reaction of H_2O with O^1D and less OH will be available for the destruction of VOCs and notably isoprene, which results in a reduced production of HCHO.

The above described sensitivity studies show that the RO_x and HCHO mixing ratios are most sensitive to the mixing ratio of NO, O_3, H_2O, CH_3OOH and isoprene. Since the measurements of isoprene and CH_3OOH have the largest uncertainty we will investigate these trace gases in more detail below.

Isoprene: Isoprene is an important precursor gas of formaldehyde and different organic peroxy radicals. The isoprene mixing ratios observed during MINATROC were high relative to the isoprene mixing ratios observed during the OCTA campaign at Izaña in July/August 1993 (Fischer et al., 1998). Excluding the measurements performed during the major dust event, the mean isoprene mixing ratio was 270±206 ppt_v during the day and below the detection limit at night. This is a factor 4.5 higher than the mean daytime isoprene mixing ratio observed during OCTA, which was 60±124 ppt_v (Fischer et al., 1998).

To study the effect of reduced isoprene mixing ratios a sensitivity run was performed in which the isoprene mixing ratios were scaled down to the mixing ratios observed during OCTA. For this simulation we divided the observed isoprene mixing ratio during MINATROC by a factor 4.5.

A reduction of the isoprene mixing ratio leads to decreases in both the HCHO and RO_x mixing ratios. The mean calc/obs ratio of RO_x decreases from 1.70 in the reference run to 1.41 in the low isoprene run. The contribution of the different peroxy radicals to the total RO_x mixing ratio changes, since less organic peroxy radicals are formed during the isoprene degradation (9%). The main constituents of RO_x are still HO_2 (65%) and CH_3O_2 (22%), while the contribution of other organic peroxy radicals decreases to 4%. The effect of isoprene on the HCHO mixing ratio is even stronger than on RO_x. The calc/obs ratio of HCHO decreases from 2.29 in the reference run to 1.49 in the low isoprene run.

Methylhydroperoxide: From the measurements with the H_2O_2 fluorescence detector an upper limit for the CH_3OOH mixing ratio could be determined. Since some major assumptions were made to infer the CH_3OOH mixing ratio, it probably has the highest uncertainty of all input parameters used in the model. CH_3OOH is an important precursor gas for HCHO and potentially has a large influence on the calculated HCHO mixing ratios. Therefore, we performed some sensitivity runs to determine the influence of methylhydroperoxide on the simulated RO_x and HCHO mixing ratios.

The CH_3OOH mixing ratio shows a similar diurnal pattern as H_2O_2; higher concentrations during the night and lower concentrations during the day. However, the difference between the day- and nighttime concentrations is much smaller than for H_2O_2. The mean CH_3OOH mixing ratio during the day was 1.0 ppb_v, comparable to the CH_3OOH mixing ratio observed in the southern hemisphere marine boundary layer (Junkermann et al., 1999; Heikes et al., 1996). It is, however, much higher than the CH_3OOH mixing ratio observed at the mountain station Mauna Loa at Hawaii (3.5 km a.s.l.), where a daytime mixing ratio of 450 ppt_v was observed during the summer (Zhou et al., 1996). Also aircraft measurements in the same altitude region show a much lower CH_3OOH mixing ratio; a mean mixing ratio of 364 ppt_v was observed between 2 and 4 km altitude over the northern Pacific Ocean (Singh et al., 2004). On the other hand, measurements in the lower free troposphere over the North American continent show a much higher median CH_3OOH mixing ratio of 1.7 ppb_v (Weinstein-Lloyd et al., 1998). Moreover, the observed mean daytime H_2O_2/CH_3OOH ratio ranged between 0.9 and 1.8 in the dust-poor airmasses, which is in agreement with the ratio observed during several other campaigns in the lower free troposphere (O'Sullivan et al., 1999). Note that the observed H_2O_2/CH_3OOH ratio in the dust plume ranged between 0.5 and 0.85, similar to the reduced ratio observed in the ITCZ region, attributed to H_2O_2 scavenging in clouds (O'Sullivan et al., 1999).

To investigate the effect of the high measurement uncertainty of CH_3OOH, a model simulation has been performed in which the input concentration of CH_3OOH has been divided by a factor of 2 compared to the reference run. Both the RO_x and HCHO mixing ratio decrease when the input CH_3OOH mixing ratio is reduced. Compared to the reference run, the calc/obs ratio of RO_x decreases from 1.70 to 1.65, while the calc/obs ratio of HCHO decreases from 2.29 to 2.16.

Isoprene and methylhydroperoxide: The estimated CH_3OOH and observed isoprene mixing ratios appear to be inconsistent with the observed RO_x and HCHO mixing ratios. Reducing the isoprene mixing ratios to values observed during a previous measurement campaign at the Izaña observatory and reducing the CH_3OOH mixing ratio to values observed at similar altitudes in the atmosphere substancially improves the agreement between the modelled and observed HCHO and RO_x mixing ratios. The results of the simulation with reduced isoprene and CH_3OOH mixing ratios are shown in Fig. 3a and b.

The modelled RO_x mixing ratio shows a smaller day to day variation compared to the observed RO_x mixing ratio. RO_x peak mixing ratios ranging from 36 to 45 pptv are calculated by the model, while the observed maximum values vary between 22 and 52 ppt_v. The model alternately under- and overestimates the midday maximum RO_x value. Considering all data points during the day, the mean ratio of the calculated RO_x mixing ratio to the observed RO_x mixing ratio (RO_x calc/obs) is 1.34, indicating an overestimation of the RO_x mixing ratio by the box model.

A detailed comparison between the observed and modelled RO_x mixing ratios is shown in Fig. 4a. Here the solid line represents the ideal 1:1 relationship between the modelled and observed values, while the dashed lines correspond to a deviation of this ideal relationship by a factor of 2, which about equals the total uncertainty of all measured parameters used as input for the model calculations. In total 304 model data points could be used for the comparison with observations, from which 97% agree within a factor of two. A straight line fit through the calculated and observed RO_x mixing ratios gives a linear correlation coefficient r of 0.58.

The diurnal variation and the absolute mixing ratios of HCHO are captured well by the model. On average the model still overestimates the HCHO mixing ratio, the mean ratio of the calculated HCHO mixing ratio to the observed HCHO mixing ratio (HCHO calc/obs) is 1.32. From the 272 data points, 99% of the calculated HCHO mixing ratios are within a factor two of the observed HCHO mixing ratios (see Fig. 4b). Moreover, a good correlation is found between the observed and calculated HCHO mixing ratios. When fitting a straight line through the data points in Fig. 4b, the correlation coefficient r is 0.84.

The HCHO mixing ratio is generally overestimated by the boxmodel, although several precursor gases, like terpenes such as α-pinene and other higher hydrocarbons (with more than 5 C-atoms), have not been included. Previous model studies using three dimensional global chemistry-transport or boxmodels have also investigated the HCHO budget. The comparison between modelled and observed HCHO concentrations provides very different results. In the remote marine boundary layer (Ayers et al., 1997; Weller et al., 2000) and the upper free troposphere (Kormann et al., 2003; Jaegle et al., 2000) models tend to underestimate the concentration of HCHO. For the marine boundary layer calculations this could at least partly be explained by a lack of higher hydrocarbons in the model, however, for the upper troposphere including higher hydrocarbons did not reproduce the high concentrations observed. For the marine boundary layer and the lower free troposphere HCHO mixing ratios are generally overestimated by models (e.g. Wagner et al., 2002; Zhou et al., 1996). Possible explanations for the overprediction of HCHO by models are deficiencies in considering dry deposition, multiphase chemistry in aerosols and clouds or halogen chemistry in the marine boundary layer. On the other hand, Olson et al. (2004) found a good agreement between observed and modelled HCHO mixing ratios between 60 and 500 ppt_v in the free troposphere. At higher HCHO concentrations the model increasingly underpredicts HCHO, which could be explained by the transport of very polluted airmasses.

HCHO dry depostion: To investigate the effect of dry deposition we included a sinusoidal dry deposition rate for HCHO analogous to H_2O_2, which is explained in detail in the next section. A noon time maximum dry deposition rate of $8.4\times10^{-7}\,\text{s}^{-1}$ is necessary to achieve good agreement between the calculated and observed HCHO mixing ratios. This is more than the dry deposition rate necessary to explain the H_2O_2 measurements (see next section). Based on the difference in solubility and reactivity, the dry deposition velocity of H_2O_2 should at least be a factor 2 higher than HCHO (L. Ganzeveld, personal communication, 2004), hence dry deposition can only partly explain the difference between model and observations.

Discussion: According to these model analyses the measured isoprene and formaldehyde mixing ratios seem to be incompatible unless a very high dry deposition rate relative to traditional deposition models is assumed. Such high deposition rates have been determined recently for other carbonyl compounds (Karl et al., 2004). Moreover, recent measurements in the Amazon basin indicate that there is biological uptake of formaldehyde in the tropical forest (Rottenberger et al., 2004). A biogenic compensation point for formaldehyde at about 600 ppt_v was found, which means that at mixing ratios below 600 ppt_v plants were found to emit formaldehyde directly, whereas for mixing ratios higher than this value, as was the case during MINATROC, direct uptake occurs. Such an uptake would distort the isoprene/formaldehyde ratios relative to a model containing only photochemistry.

The model results clearly indicate the sensitivity and direction of the model response to adjustments in the isoprene mixing ratio. Although reducing the isoprene mixing ratio does give a better fit to the modelled data, there is no instrumental indication that this measurement was erroneously high. A potential interferent at the PTR-MS mass 69 is 2-methyl-3-butenol, however, like isoprene, this species makes formaldehyde in the first oxidation step due to the terminal double bond. A recent intercomparison between this PTR-MS and both GC-FID and GC-MS systems showed very good agreement for isoprene during a measurement campaign on a forested hilltop in southern Germany (Hohenpeissenberg).

Another possibility is that the steady state assumption made in this modelling study is not valid in the case of isoprene and formaldehyde. Air advected through the adjacent forest and subsequently over the measurement site during the day may not have reached equilibrium. Therefore, the apparent incompatibility between model and measured formaldehyde may simply indicate that this assumption is not valid for this fast reacting species.

6.2.3. Simulation of hydrogen peroxide

Since we focus on the ability of the model to simulate observed H_2O_2 mixing ratios, a model simulations has been performed in which H_2O_2 is not fixed to the measured mixing ratio but has been calculated freely by the model. For this, the model run with reduced isoprene and CH_3OOH mixing ratios is taken as a reference. The results of this simulation are shown in Fig. 5. The H_2O_2 mixing ratio calculated by the model is much higher than the observed H_2O_2 mixing ratio (H_2O_2 calc/obs=2.30). This is mainly due to the fact that dry deposition of H_2O_2 at the surface is not included in the model.

The discrepancy between the calculated and observed values is largest during the Saharan dust event. Due to the high relative humidity observed during this period, relatively high H_2O_2 mixing ratios are calculated, while much lower mixing ratios were observed. Excluding the dust data points from the total dataset gives a much better agreement between observed and calculated values. For the dust-poor period, the mean calc/obs ratio of H_2O_2 is 1.89.

To improve the agreement between the observed and modelled values, we included a sinusoidal dry deposition rate for H_2O_2 in the model, with the highest deposition rate at local noon, when the upslope winds and turbulent exchange in the boundary layer are relatively strong. Dry deposition was parameterised such that after each steady state calculation the concentration of H_2O_2 was reduced according to this dry deposition rate. A calc/obs ratio of H_2O_2 of one was obtained (for the dust-poor period) when a maximum dry deposition rate of $7.1\times10^{-7}\,s^{-1}$ at local noon was assumed, corresponding to a removal fraction of 62%. For the complex meteorological situation at the measurement station with mixing of boundary layer air, which is subject to dry deposition and free tropospheric air, which is likely not influenced by dry deposition, it is difficult to translate this dry deposition rate into a deposition velocity. The results of this simulation are also presented in Figure 5. From this figure it is clear that even if dry deposition is included in the model calculations, the H_2O_2 mixing ratio is still strongly overestimated during the major Saharan dust event. A reason for this may be the uptake of H_2O_2 and/or HO_2 on the surface of the dust aerosols, which will be investigated in the next section.

6.3. Heterogeneous chemistry

The observations during the Saharan dust event show reduced mixing ratios of RO_x and H_2O_2. The reduced H_2O_2 mixing ratios could not be explained by gas phase chemistry or through the reduction in photolysis rates. Even after including dry deposition the model strongly overestimates the H_2O_2 mixing ratios during the dust event. Also the RO_x mixing ratios are overestimated by the (gas phase) model during the dust event, however, there is no clear relation with the presence of Saharan dust. To investigate the influence of Saharan dust aerosol particles on the mixing ratio of peroxy radicals and hydrogen peroxide, heterogeneous uptake reactions of HO_2 and H_2O_2 have been included in the model. Note that radiation effects of mineral dust aerosol have been accounted for by the scaling of the photolysis rates to the observed JNO_2 value.

6.3.1. Heterogeneous removal reactions

The removal rate of gas-phase species j by aerosol particles can be described by a pseudo-first-order rate coefficient k_j (s^{-1}), given by Heikes and Thompson (1983):

$$k_j = \int_{r1}^{r2} k_{d,j}(r)n(r)dr \tag{1}$$

where *n(r)dr* (cm^{-3}) represents the number concentration of particles with a radius between r and $r+dr$, and $k_{d,j}(r)$ is the size dependent mass transfer coefficient (cm^3s^{-1}), which can be calculated using the Fuchs and Sutugin (1970) interpolation equation:

$$k_{d,j} = \frac{4\pi D_j V}{1 + Kn(x + 4(1-\alpha)/3\alpha)} \tag{2}$$

where D_j (cm^2s^{-1}) is the gas phase molecular diffusion coefficient of species j, V the ventilation coefficient, which is close to unity, and Kn the dimensionless Knudsen number, defined as the ratio of the effective mean free path of a gas molecule in air, λ, to the particle radius r. α is the mass accommodation coefficient, a dimensionless number defined as the number of molecules adsorbed by the surface of an aerosol divided by the number of collisions with the aerosol; x represents a correction factor for anisotropic movement and is dependent on the Knudsen number (Fuchs and Sutugin, 1970).

In the laboratory much effort has been undertaken to determine the reactive uptake coefficient (γ) of different atmospheric gases on mineral dust aerosol (e.g. Usher et al., 2003; Hanisch and Crowley, 2003; Underwood et al., 2001). The reactive uptake coefficient represents the fraction of collisions with a particle that leads to irreversible loss of the gas (thus including chemical reactions). For the calculation of the heterogeneous removal rate the accommodation coefficient α needs to be known, denoting the probability that a gas molecule, colliding with an aerosol particle, will be (physically) incorporated into the particle. Since we do not explicitly account for chemical reactions in the condensed phase, we substitute α by γ. Since γ is a measure for the net transfer of the species to the aerosol particle, α represents an upper limit of γ.

Unfortunately no laboratory studies of the uptake of the HO_2 radical on mineral dust aerosol are documented, however, a few studies are performed to determine the uptake of HO_2 on different types of surfaces. Hanson et al. (1992), for example, determined the uptake of HO_2 on a water and sulphuric acid surface and found reactive uptake coefficients of >0.01 and >0.05, respectively, while Cooper and Abbatt (1996) measured net uptake coefficients for HO_2 radicals on supercooled sulphuric acid water-ice surfaces of 0.055 and 0.025, respectively. The presence of free Cu ions in the aerosol enhances the uptake of HO_2 on aqueous surfaces significantly (Mozurkewich et al., 1987). In a review Jacob (2000) concludes that the uptake of HO_2 by aqueous aerosols takes place with a γ of 0.1–1, and he recommends including the uptake of HO_2 by aerosols with γ=0.2 in atmospheric chemistry models. This is also the value of γ we deploy in this study. The author also concludes that although the mechanism for HO_2 uptake is uncertain, H_2O_2 is the likely product (Jacob, 2000).

Even fewer laboratory studies have been conducted on the uptake of H_2O_2 on different types of surfaces. Worsnop et al. (1989) determined the mass accommodation coefficient of H_2O_2 on aqueous surfaces. They found a strong negative temperature dependence of the mass accommodation coefficient, with an uptake coefficient of 0.18±0.02 at 273 K. Clegg and Abbatt (2001) determined the absolute uptake of H_2O_2 on an ice surface to be 4×10^9 molecules cm^{-2}, at an average ambient H_2O_2 mixing ratio of about 1 ppb$_v$. For the maximum aerosol surface area of 500 μm^2/cm^3 observed during the major Saharan dust event during MINATROC, this will cause a negligible decrease in H_2O_2 mixing ratio of much less than 1%. To our knowledge no laboratory studies on the uptake of H_2O_2 on mineral dust aerosol have been performed, therefore, different uptake coefficients will be tested in this study, starting with the value of 0.18.

The heterogeneous removal rate for HO_2 and H_2O_2 has been calculated off-line using the observed aerosol size distribution, temperature and pressure. For this, the complete size range from 6 nm to 10 μm has been taken into account.

Trajectory analyses indicate that the dust-loaded airmasses travelled about 3 days from the source region in Africa (western Algeria and Mauritania) to the measurement station. Therefore, heterogeneous removal reactions were only activated the last three days of the simulation.

6.3.2. Results of heterogeneous chemistry calculations

To find the accommodation coefficient for the heterogeneous uptake of H_2O_2 on Saharan dust particles we altered the H_2O_2 accommodation coefficient until the calc/obs ratio of H_2O_2 was equal to one. For this all data points starting at 29 July were used and dry deposition, as described in Sect. 6.2.3, was included. When the uptake coefficient for aqueous surfaces is used (γ=0.18) almost all H_2O_2 is scavenged and the calc/obs ratio of H_2O_2 decreases to 0.03. A calc/obs ratio of H_2O_2 of one was found for a much lower accommodation coefficient, 3×10^{-4}. The corresponding average removal rate of H_2O_2, k_j, during the major dust event was 5×10^{-6} s^{-1}. The results of the simulation with this accommodation coefficient are shown in Fig. 6a. From the 265 data points 93% of the modelled H_2O_2 mixing ratios were within a factor of 2 of the observed mixing ratio.

The influence of the reduced H_2O_2 mixing ratios on RO_x appears to be relatively small; the calc/obs ratio of RO_x decreases from 1.41 in the run without heterogeneous removal reactions to 1.39 in the run with H_2O_2 scavenging. Hence, the reduced RO_x mixing ratios observed during the dust event cannot be explained by heterogeneous removal of H_2O_2 on Saharan dust aerosol. Therefore, we investigated the effect of heterogeneous removal of HO_2 on Saharan dust particles on the RO_x mixing ratio. For this an uptake coefficient of 0.2 is assumed, according to the recommendation of Jacob (2000), corresponding to a first order rate coefficient, k_j, of 2×10^{-3} s^{-1} during the major dust event. Two simulations were performed: one in which the HO_2 is irreversibly removed by the dust aerosols, and one in which one molecule of H_2O_2 is produced on the surface of a dust particle for each molecule HO_2 which is taken up.

In spite of the relatively high uptake coefficient, heterogeneous removal of HO_2 causes only a small decrease in the RO_x mixing ratio. The calc/obs ratio of RO_x decreases from 1.41 in the run without heterogeneous removal reactions to 1.34 in the run with heterogeneous removal of HO_2(see Fig. 6b). Even when an uptake coefficient of 1 is assumed the model still overestimates the RO_x mixing ratio (RO_x calc/obs=1.21). The relatively small change in the calculated RO_x mixing ratio indicates that the heterogeneous removal reaction of HO_2 is slow compared to the fast gas phase production and destruction reactions of HO_2. The effect of heterogeneous removal of HO_2 on the H_2O_2 mixing ratio, however, is very strong. The H_2O_2 mixing ratio decreases to almost the observed value (H_2O_2 calc/obs=1.04) when heterogeneous removal of HO_2 with an uptake coefficient of 0.2 is included in the model. Hence, if no H_2O_2 is formed during the uptake reaction of HO_2 on Saharan dust particles, only including heterogeneous removal of HO_2 leads to a good agreement between the calculated and observed H_2O_2 mixing ratios. Note that a calc/obs ratio of H_2O_2 of exactly one is reached when heterogeneous removal of H_2O_2 with an accommodation coefficient of 7×10^{-5} is additionally included in the model.

If we assume that H_2O_2 is formed when HO_2 is taken up in the Saharan dust aerosol the H_2O_2 mixing ratio increases strongly compared to the run without heterogeneous chemistry, while the effect on RO_x is marginal. During the major dust event the calculated H_2O_2 mixing ratio exceeds 5 ppb_v, and an average calc/obs ratio of H_2O_2 of 1.92 is calculated. Heterogeneous removal of H_2O_2 with an accommodation coefficient of 1.7×10^{-3} had to be included to restore the agreement between calculated and observed values.

6.4. Ozone production rates

The model calculations have been set up to calculate the steady state concentrations of relatively short lived trace gases, while the observed mixing ratios of longer lived species, including ozone, were used as input parameters. This precludes the comparison of calculated and observed O_3 mixing ratios, and drawing conclusions about for example ozone uptake on Saharan dust particles. This would require a model calculation along a back-trajectory, however, the concentration values needed to constrain the model over the dust source region are not available.

Instead, we focus on the calculation of the net ozone production rate (NOP) during the campaign, to try to explain the low ozone mixing ratios observed during the major dust event by changes in the ozone production and loss rates. The method to determine the NOP has been introduced by Liu et al. (1980) and is summarised below. A detailed description of the procedure can also be found in Fischer et al. (2003) for the first part of the MINATROC project.

The net ozone production rate can be described as the difference between the ozone production ($PO_3=\{k_1[HO_2]+k_2[CH_3O_2]\}[NO]$) and loss rates ($LO_3=(f \times JO^1D+k_3[OH]+k_4[HO_2])\ [O_3]$), where k_1 and k_2 are the reaction rates of the reaction of NO with $HO_2$and CH_3O_2, respectively, f is the fraction of O^1D atoms reacting with H_2O to produce OH rather than being deactivated through collisions with air molecules, JO^1D is the photolysis rate of O_3, and k_3 and k_4 are the reaction rates of the reaction of O_3 with OH and HO_2, respectively. In this approach, it is assumed that ozone loss due to dry deposition, heterogeneous reactions, uptake in cloud droplets and reactions with unsaturated VOCs are negligible.

The mixing ratios of NO, O_3, H_2O (needed to calculate f) and the ozone photolysis rate were measured during MINATROC, while the OH, HO_2 and CH_3O_2 mixing ratios were calculated by the model (the run with reduced isoprene and CH_3OOH mixing ratios is used here). The net ozone production rate is shown in Fig. 7a, and ranges between 0 and 6 ppb_v/hr. During the major dust event relatively low ozone production rates are calculated. The daytime mean NOP is 0.32±0.21 ppb_v/hr during the major dust event and 1.06±1.37 ppb_v/hr in the dust-poor airmasses. The NOP is dominated by the primary production of O_3, which can be seen as a good correlation between NOP and the NO mixing ratio in Fig. 7a. This also becomes clear in Fig. 7b, where the contribution of the different production and loss processes to the NOP is shown.

The reactions of NO with HO_2 and CH_3O_2 dominate the net O_3 production rate. On the other hand, the loss terms are very small. The difference between dust-loaded and dust-poor airmasses is also determined by the difference in primary ozone production through the relatively low RO_x and NO mixing ratios in the Saharan dust airmasses.

Since the RO_x mixing ratio is overestimated by the boxmodel during the dust event, the NOP is also calculated using the measured RO_x values, maintaining the HO_2/RO_2 ratio as calculated by the boxmodel. Therefore, the modelled HO_2 and CH_3O_2 concentrations were scaled using the calc/obs ratio of RO_x. When doing so, the mean daytime NOP during the dust event decreased to 0.14±0.13 ppb_v/hr, while the NOP in the dust-poor airmasses remained the same.

The relatively low RO_x and NO mixing ratios observed during the major dust event cause a significant reduction in the net ozone production rate, however, the values remain positive. On average the difference in daytime mean O_3 mixing ratio between the dust-loaded and dust-poor airmasses was 17 ppb_v, while the difference in NOP was 0.74 and 0.92 ppb_v/hr for the modelled and observed RO_x mixing ratios, respectively. Within 23 and 18 h of sunlight, respectively, a difference of 17 ppb_v O_3 could be achieved, which corresponds to an air mass "age" of 2 to 3 days (assuming 10 h sunshine per day), which is close to the estimated age of the dust-loaded airmasses. However, since the ozone mixing ratios observed in the dust-loaded airmasses are relatively low, a net ozone production of 0.14–0.32 ppb_v/hr during the last three days would mean that the O_3 mixing ratio in the source region was even lower, about 25–30 ppb_v. The low O_3 mixing ratio observed in the dust-loaded airmasses would then be attributed to the transport of O_3 poor air from the North African continent to the measurement site. On the other hand, the relatively high NO mixing ratios observed at the measurement site are at least partly due to transport from the local boundary layer, and probably not representative for the NO mixing ratio during the last three days, which means that the airmass may have been subject to net ozone destruction during the first 2–2.5 days of its transport from the North African continent. Another possible cause for the low O_3 mixing ratios observed during the Saharan dust event is heterogeneous removal of O_3 on Saharan dust aerosol. Ozone destruction at the surface and cloud uptake could be important at this measurement site as well, however, it probably did not cause the difference between the O_3 mixing ratio observed in the dust-loaded and dust-poor air masses, since the cloud and surface conditions did not change during the campaign.

Due to the relatively high NO mixing ratios observed on several days during the MINATROC campaign, the average net ozone production rate is high compared to other campaigns. The daily average NOP ranged between 0.16 and 3.7 ppb_v/hr, and the corresponding daily average NO mixing ratio was between 27 and 265 ppt_v. During the first MINATROC campaign at Mt. Cimone the daytime mean NOP ranged between −0.1 and 0.3 ppb_v/hr for an average daily mean NO mixing ratio of about 40 ppt_v (Fischer et al., 2003), comparable to the days with lower NO mixing ratios at Izaña. At Mauna Loa, a mountain station at about the same latitude as Izaña, being much further away from pollution sources, net ozone destruction was found. During the summer of 1992 an average midday NOP of −0.15 ppb_v/hr was calculated at an average NO mixing ratio of 19 ppt_v (Cantrell et al., 1996).

7. Summary and conclusions

During the Saharan dust event reduced mixing ratios of O_3, RO_x, NO_x and H_2O_2 were observed compared to the rest of the campaign. The daytime mean O_3, NO_x and H_2O_2 mixing ratios dropped by 33%, 35% and 48% during the dust event, respectively, while the midday maximum RO_x mixing ratio decreased by 47% compared to the dust-poor days.

Using the MECCA chemistry box model, steady state concentrations of RO_x, HCHO and H_2O_2 were simulated and compared to the observed mixing ratios. The observed RO_x mixing ratios could be reproduced within a factor of two of the observed values, however, the variability of the modelled values was much lower than the variability in the observed mixing ratios. The calculated RO_x mixing ratio appeared to be rather insensitive to changes in the input concentrations of most trace gases, except for H_2O and O_3, which were constrained to the measured values in the model. Although the RO_x mixing ratios were overestimated during the major dust event, no clear relation to the presence of dust aerosol could be found.

The HCHO mixing ratio is significantly overestimated by the model, which could at least partly be explained by the neglect of dry deposition. The calculated HCHO mixing ratio is very sensitive to the input concentrations of isoprene and CH_3OOH, which are both subject to large measurement uncertainties. The model calculations indicate that the estimated CH_3OOH and observed isoprene mixing ratios may have been too high. However, we cannot finally exclude the possibility of an underestimation of the observed HCHO mixing ratios.

The observed H_2O_2 mixing ratios could only be reproduced with the box model when dry deposition was included. However, even after including dry deposition, the H_2O_2 mixing ratios were strongly overestimated during the Saharan dust event. A much better agreement between the observed and calculated H_2O_2 mixing ratios could be achieved by adding heterogeneous removal reactions of HO_2 and H_2O_2. A relatively low H_2O_2 accommodation coefficient of 3×10^{-4} was sufficient to reproduce the observed H_2O_2 mixing ratios during the dust event. Good agreement between the model and observations was also obtained by considering heterogeneous removal of HO_2 with an accommodation coefficient of 0.2. However, if we assume that H_2O_2 is formed during the heterogeneous reaction of HO_2 on mineral dust aerosol, heterogeneous removal of HO_2 had to be compensated with heterogeneous removal of H_2O_2 with a higher accommodation coefficient (1.7×10^{-3}) to obtain a good agreement between the modelled and observed values. Given that the measurements clearly indicate the uptake of HO_2 and/or H_2O_2 on Saharan dust aerosol, laboratory studies of the uptake of HO_2 and H_2O_2 on mineral dust aerosol are needed.

The low ozone mixing ratios observed during the Saharan dust event cannot be analysed with the boxmodel without making assumptions on the concentrations of O_3 and other trace gases in the dust source area. Therefore, we calculated the net ozone production rate for dust-loaded and dust-poor airmasses. Due to the relatively low RO_x and NO mixing ratios in the Saharan dust plume the NOP is significantly reduced compared to the dust-poor airmasses, which may explain the difference in O_3 mixing ratios observed in those airmasses. However, heterogeneous removal of O_3 on Saharan dust particles cannot be excluded. An average net ozone production rate of 0.14 ppb_v/hr has been calculated within the dust plume when the observed RO_x mixing ratios were used and 0.32 ppb_v/hr when the calculated RO_x mixing ratios were used. The daily average NOP ranged between 0.16 and 3.7 ppb_v/hr in the dust-poor airmasses, while the overall average daytime NOP was 1.06 ppb_v/hr.

Acknowledgements. We would like to thank E. Cuevas and his team for their technical support at the Izaña observatory and A. Kerkweg for her help with the modelling. The MINATROC project was financially supported by the European Commission (DG XII).

References

Ayers, G. P., Gillet, R. W., Granek, H., de Serves, C., and Cox, R. A.: Formaldehyde production in clean marine air, Geophys. Res. Lett., 24, 401–404, 1997.

Bauer, S. E., Balkanski, Y., Schulz, M., and Haughlustaine, D. A.: Global modeling of heterogeneous chemistry on mineral aerosol surfaces: Influence on tropospheric ozone chemistry and comparison to observations, J. Geophys. Res., 109, D02304, doi:10.1029/2003JD003868, 2004.

Bian, H. and Zender, C. S.: Mineral dust and global tropospheric chemistry: Relative roles of photolysis and heterogeneous uptake, J. Geophys. Res., 108, D21, 4672, doi:10.1029/2002JD003143, 2003.

Bonasoni, P., Cristofanelli, P., Calzolari, F., Bonafe, U., Evangelisti, F., Stohl, A., Zauli Sajani, S., van Dingenen, R., Colombo, T., and Balkanski, Y.: Aerosol-ozone correlations during dust transport episodes, Atmos. Chem. Phys., 4, 1201–1215, 2004, SRef-ID: 1680-7324/acp/2004-4-1201.

Cantrell, C. A., Shetter, R. E., Gilpin, T. M., and Calvert, J. G.: Peroxy radicals measured during Mauna Loa Observatory Photochemistry Experiment 2: The data and first analyses, J. Geophys. Res., 101, 14 643–14 652, 1996.

Carslaw, N., Plane, J. M. C., and Coe, H.: Observations of the nitrate radical in the free troposphere at Izaña de Tenerife, J. Geophys. Res., 102, 10 613–10 622, 1997.

Clegg, S. M. and Abbatt, J. P. D.: Uptake of gas-phase SO_2 and H_2O_2 by ice surfaces: dependence on partial pressure, temperature and surface acidity, J. Phys. Chem. A., 105, 6630–6636, 2001.

Cooper, P. L. and Abbatt, J. P. D.: Heterogeneous interactions of OH and HO_2 radicals with surfaces characteristic of atmospheric particulate matter, J. Phys. Chem., 100, 2249–2254, 1996.

Crutzen, P. J. and Arnold, F.: Nitric-acid cloud formation in the cold Antarctic stratosphere – a major cause for the springtime ozone hole, Nature, 324, 651–655, 1986.

Dentener, F. J., Carmichael, G. R., Zhang, Y., Lelieveld, J., and Crutzen, P. J.: Role of mineral aerosol as a reactive surface in the global troposphere, J. Geophys. Res., 101, 22 869–22 889, 1996.

de Reus, M., Dentener, F., Thomas, A., Borrmann, S., Ström, J., and Lelieveld, J.: Airborne observations of dust aerosol over the North Atlantic Ocean during ACE-2: indications for heterogeneous ozone destruction, J. Geophys. Res., 105, 15 263–15 275, 2000.

Fischer, H., Niktas, C., Parchatka, U., Zenker, T., Harris, G. W., Matuska, P., Schmitt, R., Mihelcic, D., Muesgen, P., Paetz, H. W., Schultz, M., and Volz-Thomas, A.: Trace gas measurements during the Oxidizing Capacity of the Tropospheric Atmosphere campaign 1993 at Izana, J. Geophys. Res., 103, 13 505–13 518, 1998.

Fischer, H., Kormann, R., Klüpfel, T., Gurk, Ch., Königstedt, R., Parchatka, U., Mühle, J., Rhee, T. S., Brenninkmeijer, C. A. M., Bonasoni, P., and Stohl, A.: Ozone production and trace gas correlations during the June 2000 MINATROC intensive measurement campaign at Mt. Cimone, Atmos. Chem. Phys., 3, 725–738, 2003, SRef-ID: 1680-7324/acp/2003-3-725.

Fuchs, N. A. and Sutugin, A. G.: Highly Dispersed Aerosols, Butterworth-Heinemann, Woburn, Mass., 105, 1970.

Gros, V., Williams, J., van Aardenne, J. A., Salisbury, G., Hofmann, R., Lawrence, M. G., von Kuhlmann, R., Lelieveld, J., Krol, M., Berresheim, H., Lobert, J. M., and Atlas, E.: Origin of anthropogenic hydrocarbons and halocarbons measured in the summertime European outflow (on Crete in 2001), Atmos. Chem. Phys., 3, 1223–1235, 2003, SRef-ID: 1680-7324/acp/2003-3-1223.

Hanisch, F. and Crowley, J. N.: Ozone decomposition on Saharan dust: an experimental investigation, Atmos. Chem. Phys., 3, 199–130, 2003.

Hanke, M., Umann, B., Ueker, J., Arnold, F., and Bunz, H.: Atmospheric measurements of gas-phase HNO_3 and SO_2 using chemical ionization mass spectrometry during the MINATROC field campaign 2000 on Mont Cimone, Atmos. Chem. Phys., 3, 417–436, 2003, SRef-ID: 1680-7324/acp/2003-3-417.

Hanson, D. R., Burkholder, J. B., Howard C. J., and Ravishankara, A. R.: Measurement of OH and HO_2 radical uptake coefficients on water and sulphuric acid surfaces, J. Phys. Chem., 96, 4979–4985, 1992.

Heikes, B. G. and Thompson, A. M.: Effects of heterogeneous processes on NO_3, HONO and HNO_3 chemistry in the troposphere, J. Geophys. Res., 88, 10 883–10 895, 1983.

Heikes, B., Lee, M., Jacob, D., Talbot, R., Bradshaw, J., Singh, H., Blake, D., Anderson, B., Fuelberg, H., and Thompson, A. M.: Ozone, hydroperoxides, oxides of nitrogen, and hydrocarbon budgets in the marine boundary layer over the South Atlantic, J. Geophys. Res., 101, 24 221–24 234, 1996.

IPCC (Intergovernmental Panel on Climate Change): Climate change 1995, edited by: Houghton, J. T., Meira Filho, L. G., Callender, B. A., Harris, N., Kattenberg, A., and Maskell, A., Cambridge University Press, Cambridge, UK, 572, 1996.

Jacob, D. J.: Heterogeneous chemistry and tropospheric ozone, Atmos. Environ., 34, 2131–2159, 2000.

Jaeglé, L., Jacob, D. J., Brune, W. H., Faloona, I., Tan, D., Heikes, B. G., Kondo, Y., Sachse, G. W., Anderson, B., Gregory, G. L., Singh, H. B., Pueschel, R., Ferry, G., Blake, D. R., and Shetter, R. E.: Photochemistry of Hox in the upper troposphere at northern latitudes, J. Geophys. Res., 105, 3877–3892, 2000.

Junkermann, W. and Stockwell, W. R.: On the budget of photooxidants in the marine boundary layer of the tropical South Atlantic, J. Geophys. Res., 104, 8039–8046, 1999.

Karl, T., Potosnak, M., Guenther, A., Clark, D., Walker, J., Herrick, J. D., and Geron, C.: Exchange processes of volatile organic compounds above a tropical rain forest: Implications for modelling tropospheric chemistry above dense vegetation, J. Geophys. Res., 109, D18, doi:10.1029/2004JD004738, 2004.

Kormann, R., Fischer, H., de Reus, M., Lawrence, M., Bruhl, C., von Kuhlmann, R., Holzinger, R., Williams, J., Lelieveld, J., Warneke, C., de Gouw, J., Heland, J., Ziereis, H., and Schlager, H.: Formaldehyde over the eastern Mediterranean during MINOS: Comparison of airborne in-situ measurements with 3D-model results, Atmos. Chem. Phys., 3, 851–861, 2003, SRef-ID: 1680-7324/acp/2003-3-851.

Lazrus, A. L., Kok, G. L., Lind, J. A., Gitlin, S. N., Heikes, B. G., and Shetter, R. E.: Automated fluorometric method for hydrogen-peroxide in air, Anal. Chem., 58, 594–597, 1986.

Lelieveld, J. and Crutzen, P. J.: Influences of cloud photochemical processes on tropospheric ozone, Nature, 343, 227–233, 1990.

Lelieveld, J., van Aardenne, J., Fischer, H., de Reus, M., Williams, J., and Winkler, P.: Increasing ozone over the Atlantic Ocean, Science, doi:10.1126/science.1096777, 2004.

Lindinger, W., Hansel, A., and Jordan, A.: On-line monitoring of volatile organic compounds at pptv levels by means of Proton-Transfer-Reaction Mass Spectrometry (PTR-MS): Medical applications, food control and environmental research, Int. J. Mass Spectrom. Ion Processes, 173, 191–241, 1998.

Liu, S. C., Kley, D., McFarland, M., Mahlmann, J. D., and Levi, H.: On the origin of tropospheric ozone, J. Geophys. Res., 85, 7546–7552, 1980.

Madronich, S. and Flocke, S.: The role of solar radiation in atmospheric chemistry, in: Handbook of Environmental Chemistry, edited by: Boule, P., Springer-Verlag, Heidelberg, 1–26, 1998.

Mozurkewich, M., McMurry, P. H., Gupta, A., and Calvert, J. G.: Mass accommodation coefficient for HO_2 radicals on aqueous particles, J. Geophys. Res., 92, 4163–4170, 1987.

Novelli, P. C., Masarie, K. A., Lang, P. M., Hall, B. D., Myers, R. C., and Elkins, J. W.: Reanalyisis of tropospheric CO trends: Effects of the 1997–1998 wildfires, J. Geophys. Res., 108, D15, 4464, doi:10.1029/2002JD003031, 2003.

Olson, J. R., Crawford, J. H., Chen, G., Fried, A., Evans, M. J., Jordan, C. E., Sandholm, S. T., Davis, D. D., Anderson, B. E., Avery, M. A., Barrick, J. D., Blake, D. R., Brune, W. H., Eisele, F. L., Flocke, F., Harder, H., Jacob, D. J., Kondo, Y., Lefer, B. L., Martinez, M., Mauldin, R. L., Sachse, G. W., Shetter, R. E., Singh, H. B., Talbot, R. W., and Tan, D.: Testing fast photochemical theory during TRACE-P based on measurements of OH, HO_2 and CH_2O, J. Geophys. Res., 109, D15S10, doi:10.1029/2003JD004278, 2004.

O'Sullivan, D. W., Heikes, B. G., Lee, M., Chang, W., Gregory, G. L., Blake, D. R., and Sachse, G. W.: Distribution of hydrogen peroxide and methylhydroperoxide over the Pacific and South Atlantic Oceans, J. Geophys. Res., 104, 5635–5646, 1999.

Rottenberger, S., Kuhn, U., Wolf, A., Schebeske, G., Oliva, S. T., Tavares, T. M., and Kesselmeier, J.: Exchange of short-chain aldehydes between Amazonian vegetation and the atmosphere, Ecological Applications, 14 (4), S247–S262, 2004.

Salisbury, G., Williams, J., Holzinger, R., Gros, V., Mihalopoulos, N., Vrekousis, M., Sarda-Esteve, R., Berresheim, H., von Kuhlmann, R., Lawrence, M., and Lelieveld, J.: Ground-based PTR-MS measurements of reactive organic compounds during the MINOS campaign in Crete, July–August 2001, Atmos. Chem. Phys., 3, 925–940, 2003, SRef-ID: 1680-7324/acp/2003-3-925.

Sander, R., Kerkweg, A., Jöckel, P., and Lelieveld, J.: Technical Note: The new comprehensive atmospheric chemistry module MECCA, Atmos. Chem. Phys. Discuss., 4, 7167–7180, 2004, SRef-ID: 1680-7375/acpd/2004-4-7167.

Sander, S. P., Finlayson-Pitts, B. J., Friedl, R. R., Golden, D. M., Huie, R. E., Kolb, C. E., Kurylo, M. J., Molina, M. J., Moortgat, G. K., Orkin, V. L., and Ravishankara, A. R.: Chemical Kinetics and photochemical data for use in atmospheric studies, Evaluation number 14, JPL Publications 02-25, Jet Propulsion Laboratory, Pasadena, CA, 2003.

Schultz, M.: Die Bedeutung von Stickoxiden für die Ozonbilanz in Reinluftgebieten, Untersuchung der Photochemie in Reinluft anhand von Spurengasmessungen auf Teneriffa, PhD thesis, Bergische Universität Wuppertal, Germany, 185, 1995.

Singh, H. B., Salas, L. J., Chatfield, R. B., Czech, E., Fried, A., Walega, J., Evans, M., Field, B. D., Jacob, D. J., Blake, D., Heikes, B., Talbot, R., Sachse, G., Crawford, J. H., Avery, M. A., Sandholm, S., and Fuelberg, H.: Analysis of the atmospheric distribution, sources, and sinks of oxygenated volatile organic chemicals based on measurements over the Pacific during TRACE-P, J. Geophys. Res., 109, D15S07, doi:10.1029/2003JD003883, 2004.

Tang, Y., Carmichael, G. R., Kurata, G., Uno, I., Weber, R. J., Song, C. H., Guttikunda, S. K., Woo, J. H., Streets, D. G., Wei, C., Clarke, A. D., Huebert, B., and Anderson, T. L.: Impacts of dust on regional tropospheric chemistry during the ACE-Asia experiment: A model study with observations, J. Geophys. Res., 109, D19S21, doi:10.1029/2003JD003806, 2004.

Underwood, G. M., Li, P., Al-Abadleh, H., and Grassian, V. H.: A Knudsen cell study of the heterogeneous reactivity of nitric acid on oxide and mineral dust particles, J. Phys. Chem. A, 105, 6609–6620, 2001.

Usher, C. R., Michel, A. E., and Grassian, V. H.: Reactions on mineral dust, Chem. Rev., 103, 4883–4939, 2003.

von Kuhlmann, R., Lawrence, M. G., Crutzen, P. J., and Rasch, P. J.: A model for studies of tropospheric ozone and non-methane hydrocarbons: Model description and ozone results, J. Geophys. Res., 108, D9, doi:10.1029/2002JD002893, 2003.

Wagner, V., von Glasow, R., Fischer, H., and Crutzen, P. J.: Are CH_2O measurements in the marine boundary layer suitable for testing the current understanding of CH_4 photooxidation?: A model study, J. Geophys. Res., 107, D3, doi:10.1029/2001JD000722, 2002.

Weinstein-Lloyd, J. B., Lee, J. H., Daum, P. H., Kleinman, L. I., Nunnermacker, L. J., Springston, S. R., and Newman, L.: Measurements of peroxides and related species during the 1995 summer intensive of the Southern Oxidants Study in Nashvill, Tennessee, J. Geophys. Res., 103, 22 361–22 373, 1998.

Weller, R., Schrems, O., Boddenberg, A., Gäb, S., and Gautrois, M.: Meridional distribution of hydroperoxides and formaldehyde in the marine boundary layer of the Atlantic (48° N–35° S) measured during the Albatross campaign, J. Geophys. Res., 105, 14 401–14 412, 2000.

Williams, J., Pöschl, U., Crutzen, P. J., Hansel, A., Holzinger, R., Warneke, C., Lindinger, W., and Lelieveld, J.: An atmospheric chemistry interpretation of mass scans obtained from a proton transfer mass spectrometer flown over the tropical rainforest of Surinam, J. Atmos. Chem., 38, 133–166, 2001.

Worsnop, D. R., Zahniser, M. S., Kolb, C. E., Gardner, J. A., Watson, L. R., Van Doren, J. M., Jayne, J. T., and Davidovits, P.: Temperature dependence of mass accommodation of SO_2 and H_2O_2 on aqueous surfaces, J. Phys. Chem., 93, 1159–1172, 1989.

Zaveri, R. A., Saylor, R. D., Peters, L. K., McNider, R., and Song, A.: A model investigation of summertime diurnal ozone behaviour in rural mountainous locations, Atmos. Environ., 29, 1043–1065, 1995.

Zhang, Y. and Carmichael, G. R.: The role of mineral aerosol in tropospheric chemistry in East Asia – a model study, J. Appl. Meteorol., 38, 353–366, 1999.

Zhang, Y., Sunwoo, Y., Kotamarthi, V., and Carmichael, G. R.: Photochemical oxidant processes in the presence of dust: an evaluation of the impact of dust on particulate nitrate and ozone formation, J. Appl. Meteorol., 33, 813–824, 1994.

Zhou, X., Lee, Y. N., Newman, L., Chen, X., and Mopper, K.: Tropospheric formaldehyde concentrations at the Mauna Loa Observatory during the Mauna Loa Observatory Photochemistry Experiment 2, J. Geophys. Res., 101, 14 711–14 719, 1996.

Table 1. Instrumentation used for trace gas measurements during MINATROC.

Species	Measurement principle	Instrument	Uncertainty	Detection limit
O_3	UV absorption	Ansyco 41M	<5%	1 ppb_v
CO	Gas chromatograph	Thermo-Electron	5%	
NO	chemiluminescence detector (CLD)	ECOPHYSICS CLD 790SR	3%	8 ppt_v
NO_2	CLD and photolytic converter (PLC)	ECOPHYSICS CLD 790SR and PLC 760	8% at night, 20% during the day	24 ppt_v
NO_y	CLD and catalytic converter	ECOPHYSICS CLD 770AL	5.6%	100 ppt_v
HCHO	Fluorescence detector (Hantzsch reaction)	Aero Laser AL4021	5%	23 ppt_v
H_2O_2	Fluorescence detector (dual enzyme technique)	Aero Laser AL2001CA	20%	60 ppt_v
CH_3OOH	Fluorescence detector	AL2001CA	100%[1]	60 ppt_v
RO_x	Chemical amplifier and photoluminescence detector	PERCA and Luminox LMA-3	30–40%	2 ppt_v
Acetone, methanol, isoprene	Proton-Transfer-Reaction Mass Spectrometer (PTRMS)		<28%	55 ppt_v, 213 ppt_v, 46 ppt_v
Propane, butane	Gas chromatograph-mass spectrometer (GC-MS)	Agilent GC-MS 6890/5973	<15%	3 ppt_v
JO^1D	Filter Radiometer	METCON	20%[2]–30%[3]	$8{\cdot}10^{-7}\ \mathrm{s}^{-1}$
JNO_2	Filter Radiometer	METCON	10%[2]–20%[3]	$8{\cdot}10^{-7}\ \mathrm{s}^{-1}$

[1] Estimated uncertainty for the CH_3OOH measurements, see text.

[2] For solar zenith angles<60°

[3] For solar zenith angles between 60° and 70°

Table 2. Average values for meteorological parameters, trace gas mixing ratios and aerosol properties (aerosol number concentration (N), surface area (A), volume (V) and mass) observed during the Saharan dust event and for the dust-poor airmasses. The dataset is subdivided in daytime (upslope) and nighttime (downslope) conditions.

	Daytime		Nighttime	
	low dust	high dust	low dust	high dust
Temperature (°C)	18.2±3.5	20.0±1.6	15.8±3.3	17.2±1.6
RH (%)	19±11	35±13	16±12	37±15
CO (ppb_v)	96±27	92±6	87±29	87±3
O_3 (ppb_v)	52±12	35±6	58±15	36±3
HCHO (ppb_v)	0.65±0.32	0.64±0.14	0.29±0.08	0.47±0.16
H_2O_2 (ppb_v)	1.24±0.38	0.64±0.28	1.72±0.55	0.61±0.25
CH_3OOH (ppb_v)[1]	1.0±0.26	0.93±0.16	1.1±0.34	0.99±0.21
NO_x (ppb_v)	0.26±0.20	0.17±0.07	0.10±0.04	0.11±0.05
NO_y (ppb_v)	1.14±0.75	0.74±0.24	0.77±0.38	0.51±0.20
RO_x (ppt)[2]	43±16	28±6	–	–
Methanol (ppb_v)	2.35±0.66	2.8±0.5	1.40±0.43	2.3±0.8
Acetone (ppb_v)	1.34±0.31	1.4±0.13	1.05±0.23	1.3±0.24
Isoprene (ppb_v)	0.27±0.21	0.35±0.26	0.03±0.02	0.05±0.02
Propane (ppt_v)	41±25	38±15	22±11	34±18
Butane (ppt_v)	35±37	15±6	13±31	24±28
N (cm^{-3})	1463±2451	551±230	261±186	364±119
A (μm^2 cm^{-3})	27±23	152±86	16±16	155±54
V (μm^3 cm^{-3})	3.8±4.1	50±29	3.4±4.7	55±19
Mass (μg m^{-3})	13±14	186±116	12±16	199±61

---

[1] The CH_3OOH given here is an upper limit for the atmospheric CH_3OOH mixing ratio.

[2] For RO_x the average daytime maximum mixing ratio is given.

Table 3. Comparison of the median daytime and nighttime (day/night) trace gas mixing ratios during the MINATROC campaign at Izaña and at Mt. Cimone and during the OCTA campaign at Izaña in July/August 1993. For RO_x only a mean noontime value is given. Only the dust-poor data from MINATROC is used for this comparison.

	Izaña	Mt. Cimone[1]	Izaña[2]
Field campaign	MINATROC	MINATROC	OCTA
Time period	July/August 2002	June 2000	July/August 1993
O_3 (ppb_v)	52/59	56/60	38/40
CO (ppb_v)	88/78	119/118	92/89
NO_x (ppt_v)	210/95	267/197	76/47
NO_y (ppb_v)	0.95/0.66	0.90/1.0	0.52/0.39
HCHO (ppb_v)	0.58/0.29	1.4/1.1	1.4/1.1
H_2O_2 (ppb_v)	1.17/1.63	n.a.	2.1/2.4
RO_x (ppt_v)	43	31	65

[1] Fischer et al. (2003)

[2] Fischer et al. (1998)

Table 4. Calculated RO_x and HCHO mixing ratios and calculated/observed ratios for the sensitivity runs in which the mixing ratio of the trace gas in column 1 has been reduced by a factor 2 compared to the reference run.

	RO_x (ppt_v)	RO_x calc/obs	HCHO (ppb_v)	HCHO calc/obs
Reference run	40	1.70	1.81	2.29
O_3	36	1.52	1.63	2.03
CO	41	1.72	1.86	2.34
H_2O	37	1.58	1.69	2.12
NO	38	1.62	1.22	1.55
Methanol	40	1.70	1.80	2.27
Acetone	40	1.69	1.80	2.27
HNO_3	40	1.70	1.81	2.28
H_2O_2	40	1.67	1.79	2.25
CH_3OOH	39	1.65	1.72	2.16
Isoprene	36	1.53	1.43	1.83
NMHC	40	1.70	1.81	2.28

Title Page
Abstract | Introduction
Conclusions | References
Tables | Figures
◀◀ | ▶▶
◀ | ▶
Back | Close
Full Screen / Esc
Print Version
Interactive Discussion
EGU

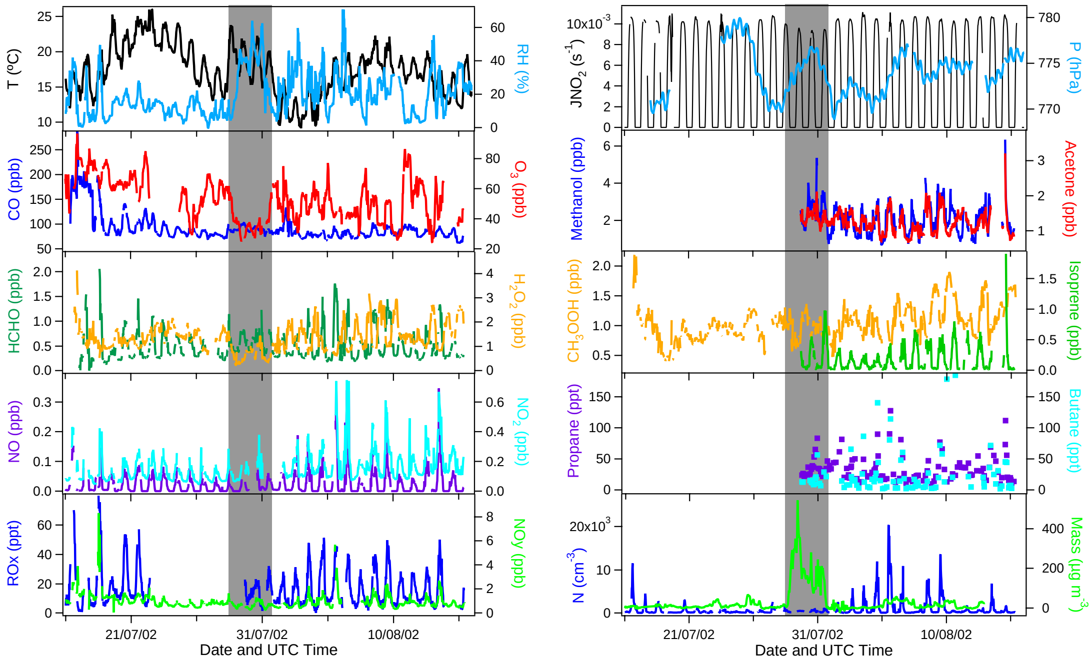

Fig. 1. Time series of the observed meteorological parameters, trace gas mixing ratios and aerosol number and mass concentrations during MINATROC. The major Saharan dust event is marked by the grey area.

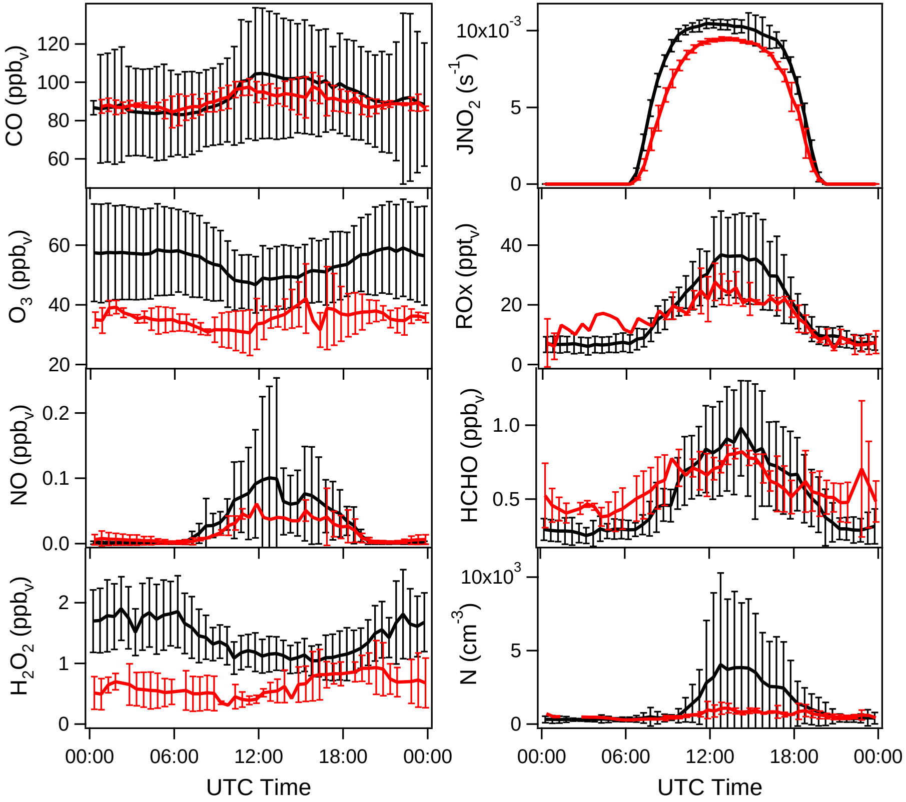

Fig. 2. Diurnal variation of a selection of trace gases and the aerosol number concentration during MINATROC. The red line represents the observations (and 1σ standard deviation) during the major Saharan dust event, the black line the data outside the dust event.

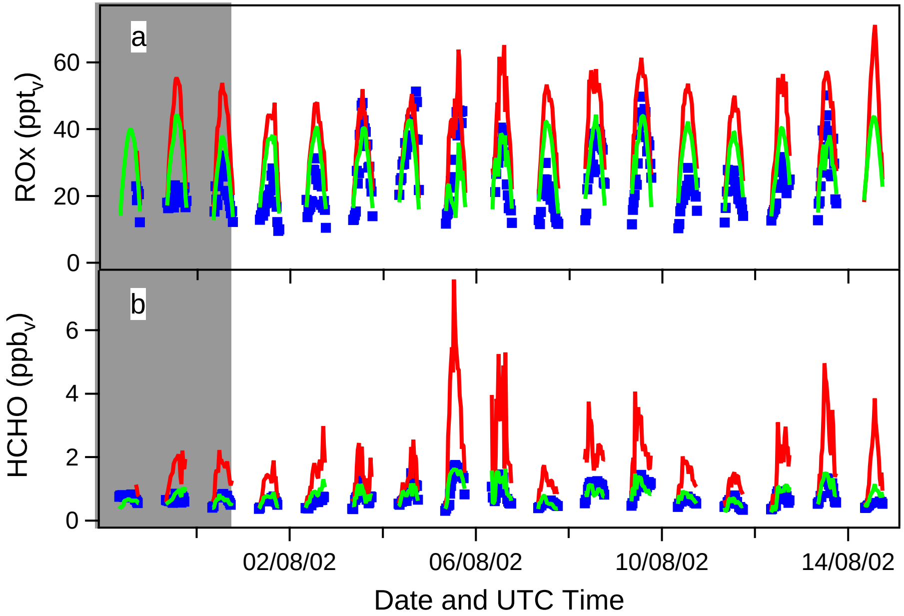

Fig. 3. Observed (blue dots) and modelled (red solid line, reference run) RO_x and HCHO mixing ratios. The green solid line represents the model calculation with reduced isoprene and CH_3OOH mixing ratios. The major Saharan dust event is marked by the grey area.

Title Page
Abstract | Introduction
Conclusions | References
Tables | Figures
◀| |▶
◀ ▶
Back | Close
Full Screen / Esc
Print Version
Interactive Discussion

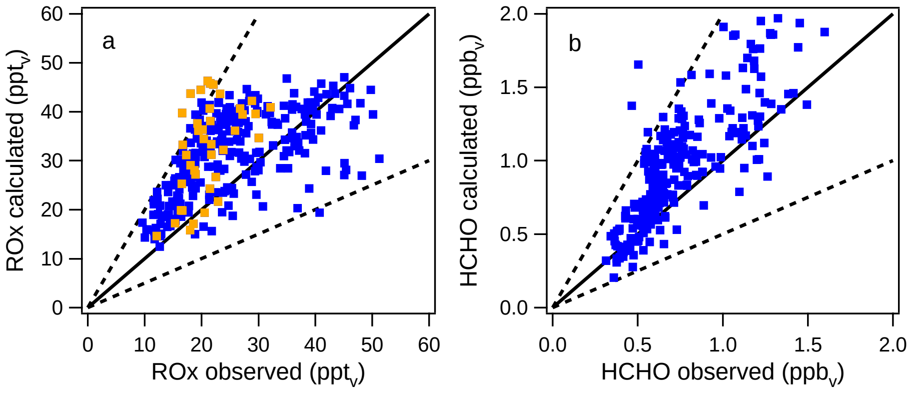

Fig. 4. Comparison between the calculated and observed RO_x **(a)** and HCHO **(b)** mixing ratios (blue dots) for the model run with reduced isoprene and CH_3OOH mixing ratios. The orange dots represent the RO_x mixing ratios during the major Saharan dust event. The solid black line represents the 1:1 relationship, the dashed lines the 1:2 and 2:1 relationships.

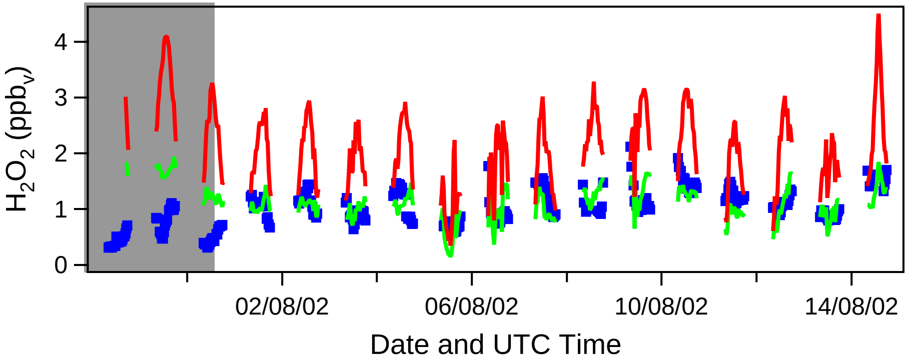

Fig. 5. Observed (blue dots) and calculated (red solid lines) H_2O_2mixing ratios for the model run in which the mixing ratios of H_2O_2 are not fixed to the observed values. The green solid line represents the model run in which dry deposition of H_2O_2 is included. The major Saharan dust event is marked by the grey area.

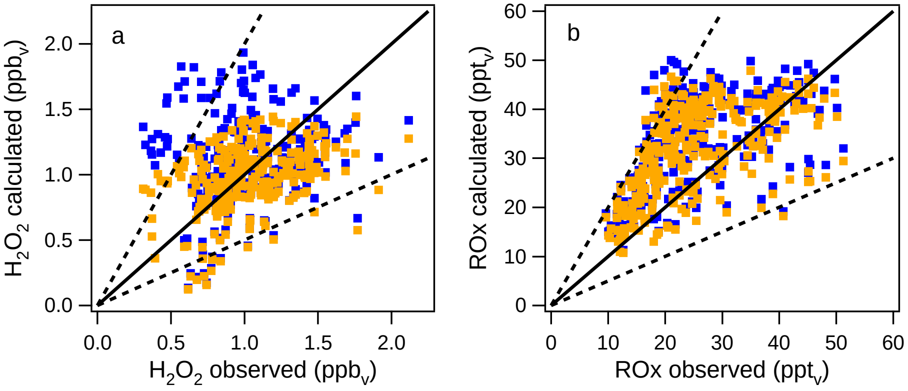

Fig. 6. Comparison between the calculated and observed H_2O_2 and RO_x mixing ratios (blue dots). The orange dots represent the model run including heterogeneous removal of **(a)** H_2O_2 ($\gamma=3\times10^{-4}$) and **(b)** HO_2 ($\gamma=0.2$) on Saharan dust aerosol. The solid black line represents the 1:1 relationship, the dashed lines the 1:2 and 2:1 relationships.

Title Page
Abstract
Introduction
Conclusions
References
Tables
Figures
◀◀
▶▶
◀
▶
Back
Close
Full Screen / Esc
Print Version
Interactive Discussion

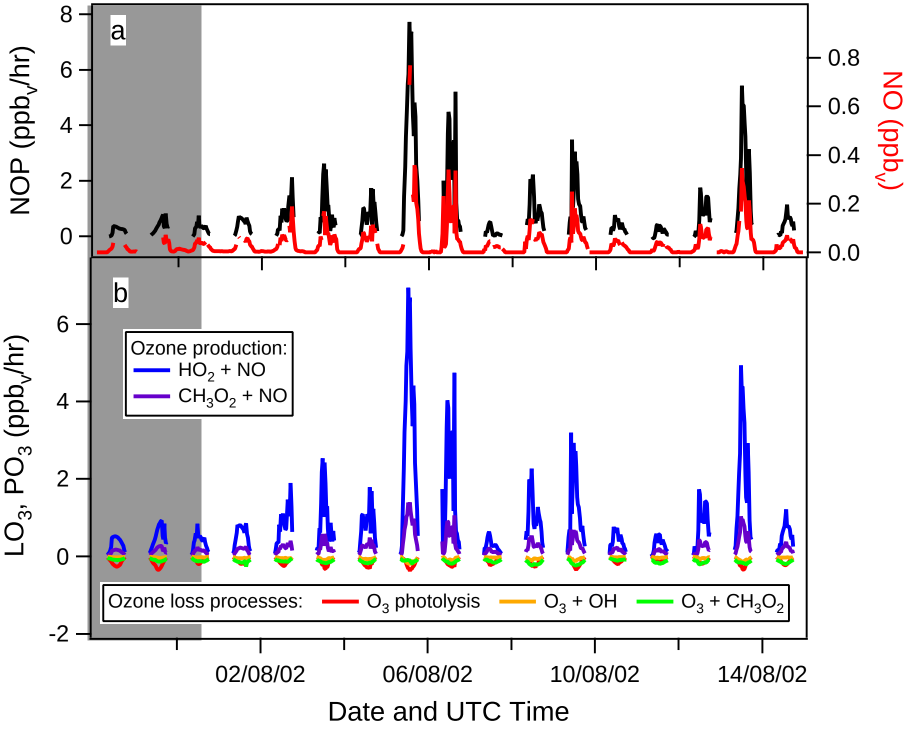

Fig. 7. Calculated net ozone production rate (NOP) for the MINATROC campaign **(a)** and partitioning of the different production and loss processes **(b)**. The major Saharan dust event is marked by the grey area.